

## MAPPING NEUTRAL HYDROGEN DURING REIONIZATION WITH THE Ly $\alpha$ EMISSION FROM QUASAR IONIZATION FRONTS

SEBASTIANO CANTALUPO, CRISTIANO PORCIANI AND SIMON J. LILLY

Institute for Astronomy, ETH Zürich, CH-8093 Zürich, Switzerland

*To be published in the Astrophysical Journal*

### ABSTRACT

We present a new method to directly map the neutral-hydrogen distribution during the reionization epoch and to constrain the emission properties of the highest-redshift quasars (QSOs). As a tracer of HI, we propose to use the Ly $\alpha$  radiation produced by quasar ionization fronts (I-fronts) that expand in the partially ionized intergalactic medium (IGM) before reionization is complete. These Ly $\alpha$  photons are mainly generated by collisional excitations of hydrogen atoms in the boundary of the rapidly expanding HII region. The observable signal is produced by the part of the I-front that lies behind the QSO with respect to the observer. The expected Ly $\alpha$  flux depends on the properties of both the QSO (e.g. its total ionizing rate and spectral hardness) and the surrounding medium (e.g. the local density and the mean hydrogen neutral fraction). Combining two radiative transfer models (one for the QSO ionizing radiation and one for the Ly $\alpha$  photons), we estimate the expected Ly $\alpha$  spectral shape and surface brightness (SB<sub>Ly $\alpha$</sub> ) for a large number of configurations where we varied both the properties of the ionizing QSO and of the surrounding medium. We find that the expected signal is observable as a single (broad) emission line with a characteristic width of 100 – 200 km s<sup>-1</sup>. The expected SB<sub>Ly $\alpha$</sub>  produced at redshift  $z \simeq 6.5$  within a fully neutral region (at mean density) by a typical QSO I-front lies in the range  $10^{-21} - 10^{-20}$  erg s<sup>-1</sup> cm<sup>-2</sup> arcsec<sup>-2</sup> and decreases proportionally to  $(1+z)^2$  for a given QSO age. QSOs with harder spectra may produce a significantly brighter emission at early phases. The signal may cover up to a few hundred square arcmin on the sky and should be already detectable with current facilities by means of moderate/high resolution spectroscopy. The detection of this Ly $\alpha$  emission can shed new light on the reionization history, the age and the emission properties of the highest-redshift QSOs.

*Subject headings:* cosmology: theory - diffuse radiation - intergalactic medium - radiative transfer - line: profiles - quasars: general

### 1. INTRODUCTION

The epoch of reionization (EoR) marks the time at which the first luminous sources ionized the mostly neutral intergalactic medium (IGM). Uncovering when and how the EoR took place represents one of the most fundamental questions of modern cosmology and considerable efforts are being made to understand this era.

The recent polarization measurements of the cosmic microwave background (CMB) by the WMAP satellite suggest that the universe was mostly neutral at redshift  $z \gtrsim 14$  (Page et al. 2006). On the other hand, at  $z < 5$ , hydrogen absorption features in the spectra of luminous quasars are resolved into individual Ly $\alpha$  forest lines (e.g. Rauch 1998) as expected in a highly ionized IGM. At  $z \gtrsim 6$ , quasar spectra start showing complete Gunn-Peterson absorption troughs (GPT) which might suggest a rapid increase in the neutral fraction of cosmic hydrogen (Becker et al. 2001; Fan et al. 2003; White et al. 2003). However, the Ly $\alpha$  transition has a large cross-section and the presence of GPTs only requires very low values for mean neutral fraction of cosmic hydrogen:  $\langle x_{HI} \rangle \gtrsim 10^{-3}$  (Fan et al. 2002; Songaila 2004; Oh & Furlanetto 2005).

Stronger constraints on  $\langle x_{HI} \rangle$  can be obtained from the detailed spectral shape of the GPT, i.e. from the size of the HII region produced by the QSO itself (White et al. 2003; Mesinger & Haiman 2004; Wyithe & Loeb 2004; Yu

& Lu 2005; Fan et al. 2006; Maselli et al. 2006; Bolton & Haehnelt 2007). The physical scales of these regions are typically inferred to be  $\sim 5$  Mpc at  $z > 6$  (Fan et al. 2006), an order of magnitude larger than the HII bubbles expected from clustered star-forming galaxies (Furlanetto, Zaldarriga & Hernquist 2004). The size of the HII region around a QSO depends on the neutral density of the surrounding medium but also on the source luminosity and age (more specifically, on its light curve). With some knowledge of the QSO parameters it is then possible to constrain the value of  $\langle x_{HI} \rangle$ . Whythe et al. (2005) applied this method to seven QSOs at  $6 \lesssim z \lesssim 6.42$  and derived  $\langle x_{HI} \rangle \gtrsim 0.1$ . Similarly, from the size of the Ly $\alpha$  and Ly $\beta$  troughs of a QSO at  $z = 6.28$ , Mesinger & Haiman (2004) found  $\langle x_{HI} \rangle \gtrsim 0.2$ . On the contrary, Fan et al. (2006) did not find strong evidence for a mean hydrogen neutral fraction as high as 0.1 at  $z = 6.4$ . Apart from systematics, the main uncertainty of this method lies in the estimate of the QSO age. As a matter of fact, the current observed sizes seem to be equally consistent with both a significantly neutral and a highly ionized surrounding IGM (e.g. Bolton & Haehnelt 2007).

Additional (indirect) information about the ionized fraction of the IGM can be obtained from the luminosity-function evolution of Ly $\alpha$  emitting galaxies (LAE) at  $z > 6$  (Miralda-Escudé 1998; Madau & Rees 2000; Haiman 2002; Santos 2004; Taniguchi et al. 2005; Furlanetto et al. 2006; Malhotra & Rhoads 2006; Kashikawa et al. 2006), and from their clustering properties (McQuinn

et al. 2007). The key idea is that the observed Ly $\alpha$  flux from high- $z$  galaxies should strongly depend on the neutral fraction of their surrounding medium. However, these observations are challenging and difficult to interpret. Any change in the luminosity function due to the EoR must be distinguished from an intrinsic physical evolution of the sources, as well as the effects of dust or galactic winds. Similarly, clustering signatures of the EoR can only be detected by comparing the spatial distribution of a given galaxy population (e.g. Lyman-break galaxies) with that of the sub-sample of LAEs (see Fan, Carilli & Keating 2006 for a recent review).

A very promising method for studying the EoR is the detection of the redshifted 21-cm emission from neutral hydrogen (Madau, Meiksin & Rees 1997; see Furlanetto, Oh & Briggs 2006 for a recent and exhaustive review). This technique has received a lot of attention recently as a concrete possibility of studying the detailed history of the EoR. From the technical point of view, however, it requires an extremely challenging measure: the intrinsic 21-cm signal, detected as a brightness-temperature fluctuation against the CMB, is at least four orders of magnitude smaller than the emission from our Galaxy. Other important foregrounds include radio recombination lines, terrestrial interference and ionospheric distortion. The hope is to separate the fluctuating spectral features due to 21-cm emission from the smooth spectrum of the foregrounds. Anyway, given the difficulties of high signal-to-noise imaging, attention has been focussed on statistical measurements, like the power-spectrum analysis. First-generation facilities (as LOFAR and MWA, now under construction) should only detect a statistical signature of reionization. For a direct detection of the three-dimensional structure of HI and HII regions (the so called “21-cm tomography”) we will probably have to wait for a subsequent generation of radio arrays with much larger collecting area (e.g. SKA).

Are there other possibilities to directly detect the high- $z$  IGM in emission? Ly $\alpha$  is the strongest hydrogen emission line. This transition (from the 2P to the 1S level of atomic hydrogen) has a spontaneous emission coefficient  $A_{21} = 6.25 \times 10^8 \text{ s}^{-1}$ . An efficient mechanism to populate the  $n = 2$  level, with consequent Ly $\alpha$  emission, is the HII recombination process. Unfortunately, the recombination rate is typically very low and recombination radiation from optically thin hydrogen in the high-redshift IGM cannot be detected with current instruments (see e.g. Hogan & Weymann 1987; but also Baltz, Gnedin & Silk 1998).

Optically thick and self-shielded HI clouds exposed to strong UV radiation are expected to re-emit a significant part of the impinging flux in the form of “fluorescent” Ly $\alpha$  emission (Gould & Weinberg 1996; Cantalupo et al. 2005). A recent attempt to detect fluorescent emission, and thus HI protogalactic-clouds, at intermediate redshift ( $z \sim 3$ ) has provided a number of promising candidates (Cantalupo, Lilly & Porciani 2007). However, self-shielded clouds correspond to overdense regions with relatively small sizes that trace just a small fraction of the neutral hydrogen distribution.

Under favourable conditions, the excitation of atomic hydrogen due to collisions with energetic electrons populates the  $n = 2$  level in a much more efficient way than recombinations. In this paper, we show that the corre-

sponding Ly $\alpha$  emission can be efficiently used to map the neutral hydrogen distribution during the EoR. This emission should be already detectable with current observational facilities and could be used to shed light on the bulk of neutral hydrogen during the EoR.

The layout of the paper is as follows. In §2 we summarize the basic physics of Ly $\alpha$  emission from recombination and collisional excitation processes. In §3 we show that collisional excitations should efficiently produce Ly $\alpha$  emission within the ionization fronts of high-redshift QSOs. We also explain how it is possible to map the distribution of neutral hydrogen behind the QSO using this emission. In §4 we present more sophisticated models of Ly $\alpha$  emission based on numerical simulations including a detailed treatment of radiative transfer. In §5 we discuss the dependence of our results on model parameters and possible detection strategies. Finally, in §6, we summarize our results. The reader who is not interested into the technical details of the model can safely read §5.2 right after §3 (focussing also on Figures 7 and 8).

Throughout this paper, we adopt a standard, flat  $\Lambda$ CDM cosmological model with mass-density parameter  $\Omega_m = 0.24$ , a baryonic contribution of  $\Omega_b = 0.044$ , and a present-day Hubble constant of  $H_0 = 100 h \text{ km s}^{-1} \text{ Mpc}^{-1}$  with  $h = 0.73$ . We also adopt the notation “pMpc” to indicate proper distances measured in Mpc.

## 2. THE PHYSICS OF LY $\alpha$ EMISSION

There are two main channels that drive the production of Ly $\alpha$  photons in the IGM: i) recombination processes and ii) collisional excitations by free electrons. Both mechanisms directly arise from the ionization of the hydrogen atom.

### 2.1. Ly $\alpha$ from recombinations

When an electron is captured by a free proton, it can either directly populate the ground  $1^2S$  level (with the emission of a Lyman continuum photon) or an excited state from which it cascades by downward transitions to the  $1^2S$  level (with the emission of a continuum photon plus several transition lines). Cascades that populate the  $2^2P$  state decay to the  $1^2S$  level by emitting a Ly $\alpha$  photon, while cascades to the  $2^2S$  level subsequently decay via two-photon emission.

Electrons that populate  $n \geq 3$  levels may also decay to the ground state with the emission of another Lyman-series line (with no two-photon or Ly $\alpha$  emission). However, even in the low-density IGM, the typical Lyman-line emitting regions have quite large optical depths ( $\tau$ ) in the Lyman resonance lines (Osterbrock 1989). Therefore, a good approximation (unless the medium is fully ionized) is to assume that every Lyman-line photon from  $n \geq 3$  levels is converted into lower-series photons plus either Ly $\alpha$  or two-photon radiation (Case B approximation, Baker & Menzel 1938). In this case, it is convenient to write the effective Ly $\alpha$  emission coefficient from recombinations as:

$$\alpha_{\text{Ly}\alpha}^{\text{eff}}(T) = \epsilon_{\text{Ly}\alpha}^{\text{B}}(T)\alpha_{\text{B}}(T), \quad (1)$$

where  $\alpha_{\text{B}}(T)$  is the hydrogen total recombination coefficient excluding recombinations to the ground level, and  $\epsilon_{\text{Ly}\alpha}^{\text{B}}(T)$  is the fraction of those recombinations producing Ly $\alpha$  photons. Combining the tabulated values by

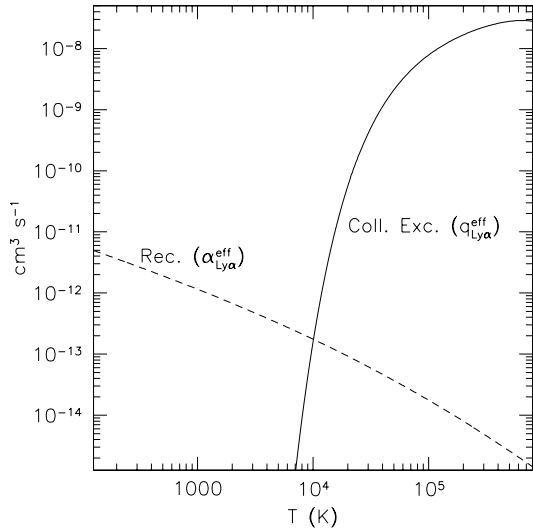


FIG. 1.— Effective Ly $\alpha$  production rate from recombination processes ( $\alpha_{\text{Ly}\alpha}^{\text{eff}}$ , dashed line) and collisional excitations ( $q_{\text{Ly}\alpha}^{\text{eff}}$ , solid line) as a function of the gas (electronic) temperature.

Pengelly (1964; for  $T > 10^3$  K) and Martin (1988; for  $T < 10^3$  K), we have derived the following fitting formula for  $\epsilon_{\text{Ly}\alpha}^{\text{B}}(T)$  (accurate to the 0.1% in the temperature range  $100 \text{ K} < T < 10^5 \text{ K}$ ):

$$\epsilon_{\text{Ly}\alpha}^{\text{B}}(T) = 0.686 - 0.106 \log(T_4) - 0.009 \cdot (T_4)^{-0.44}, \quad (2)$$

where  $T_4 = T/10^4 \text{ K}$ . Note that the value of  $\epsilon_{\text{Ly}\alpha}^{\text{B}}(T)$  varies very little with temperature, ranging between 0.68 and 0.61 for  $T_4 = 1 - 5$ . The temperature dependence of  $\alpha_{\text{Ly}\alpha}^{\text{eff}}(T)$  is shown in Figure 1 as a dashed line. Note that the value of  $\epsilon_{\text{Ly}\alpha}^{\text{B}}(T)$  varies very little with temperature, ranging between 0.68 and 0.61 for  $T_4 = 1 - 5$ .

The volume Ly $\alpha$  emissivity due to radiative recombinations is given by:

$$\frac{4\pi j_{\text{Ly}\alpha}}{h\nu_{\text{Ly}\alpha}} = n_e n_p \alpha_{\text{Ly}\alpha}^{\text{eff}} \quad (3)$$

where  $j_{\text{Ly}\alpha}$  is the emissivity (energy radiated per unit time, volume and solid angle),  $h\nu_{\text{Ly}\alpha} = 10.2 \text{ eV}$  is the energy of a Ly $\alpha$  photon and  $n_e$ ,  $n_p$  are, respectively, the electron and proton number densities. Note that the coefficient  $\alpha_{\text{Ly}\alpha}^{\text{eff}}$  is independent from the assumption regarding the fate of Lyman-continuum photons. Whenever these photons are absorbed, and also in the case they escape the medium, the local values of  $n_e$  and  $n_p$  will change accordingly, modifying the Ly $\alpha$  emissivity.

## 2.2. Ly $\alpha$ from collisional excitations

Free electrons can interact one or more times with neutral hydrogen atoms before eventually recombining. Given the relatively low densities of the IGM, we can imagine the free electrons colliding with hydrogen in the ground state and transferring to it a fraction of their energy. If this energy (i.e. the electron temperature) is high enough, the collision will excite the atomic levels with subsequent decay via line emission. The efficiency of the process is strongly temperature dependent. In particular, the collisional excitation coefficient for the transition

from the ground level (1) to the level  $nl$  is given by:

$$q_{1,nl} = \frac{8.629 \times 10^{-6} \Omega(1, nl)}{\sqrt{T} \omega_1} e^{-E_{1,n}/k_B T} \text{ cm}^3 \text{ s}^{-1}, \quad (4)$$

where  $\Omega(1, nl)$  is the temperature dependent effective collision strength,  $\omega_1$  is the statistical weight of the ground state and  $E_{1,n}$  is the energy difference between the ground and the  $nl$  level. We define the effective collisional excitation coefficient for Ly $\alpha$  emission as:

$$q_{\text{Ly}\alpha}^{\text{eff}} = q_{1,2p} + q_{1,3s} + q_{1,3d} \quad (5)$$

where we consider excitation processes up to the level  $n = 3$  that will eventually produce Ly $\alpha$  radiation (in Case B approximation). The contribution from higher levels is completely negligible for the electron temperatures we are interested in. Similarly, we neglect angular-momentum-exchanging processes from proton and electron collisions (e.g. the 2s-2p and 2p-2s transition) that, in principle, might boost or suppress Ly $\alpha$  emission. The typical densities of the IGM are too low for these transitions to be important (Osterbrock 1989). We use the polynomial fits of Giovanardi, Natta & Palla (1987) to compute  $q_{\text{Ly}\alpha}^{\text{eff}}$ . The result is shown as a solid line in Figure 1.

The total Ly $\alpha$  emissivity coming from radiative recombinations and collisional excitations is thus given by:

$$\frac{4\pi j_{\text{Ly}\alpha}}{h\nu_{\text{Ly}\alpha}} = n_e n_p \alpha_{\text{Ly}\alpha}^{\text{eff}} + n_e n_{\text{HI}} q_{\text{Ly}\alpha}^{\text{eff}}, \quad (6)$$

where  $n_{\text{HI}}$  is the neutral hydrogen density. Higher ionization fractions favour Ly $\alpha$  emission from radiative recombinations, while higher temperatures increase the contribution from collisional excitations provided that a significant fraction of hydrogen atoms remain neutral. Therefore, collisional excitation significantly contributes to the total Ly $\alpha$  emissivity in relatively hot regions where  $n_e \sim N_{\text{HI}}$ , i.e. where the neutral fraction ( $x_{\text{HI}}$ ) is about 0.5. In particular, if the temperature of these regions is in the range  $2 - 5 \times 10^4 \text{ K}$ , collisional excitation may increase the total Ly $\alpha$  signal of several orders of magnitudes with respect to radiative recombinations.

## 3. Ly $\alpha$ EMISSION FROM QUASAR IONIZATION FRONTS DURING REIONIZATION

The two requirements for efficient Ly $\alpha$  production via collisional excitation ( $T \sim$  a few  $\times 10^4 \text{ K}$  and  $x_{\text{HI}} \sim 0.5$ ) are met within the ionization fronts (I-fronts) produced by powerful UV sources with a hard spectrum (like QSOs) located in a mostly neutral IGM. An I-front constitutes the transition region between the inner HII zone and the outer (predominantly neutral) IGM. In this transition layer, the hydrogen neutral fraction varies by several orders of magnitudes within a length scale determined by the mean free path of the ionizing photons. The thickness of the I-front is generally negligible with respect to the characteristic radius of the HII region. Sources with harder spectra produce thicker I-fronts (for a given IGM density) because of the frequency dependence of the photo-ionization cross-section. If the I-front is not in photo-ionization equilibrium, ionization fractions evolve with time and the transition zone moves outward (the HII region expands). The propagation of the I-front produced by powerful UV sources like QSO can be highly

relativistic, racing ahead of the hydrodynamic response of the ionized gas for the entire lifetime of the source (Shapiro & Giroux 1987).

### 3.1. A simple estimate of the Ly $\alpha$ signal

As shown in equation (6), the volume emissivity of Ly $\alpha$  radiation within the I-front depends on the electron, proton and HI densities, and on the local temperature. Detailed modelling of these quantities within an expanding I-front requires an accurate numerical solution of the radiative transfer problem and is postponed to the next Section. However, we can give an order-of-magnitude estimate of the expected amplitude of the signal following a simple analytical reasoning.

Let us assume that a bright QSO turns on at redshift  $z_{in} > 6$ , before the reionization process is complete, and produces a rapidly expanding I-front that completely ionizes the surrounding IGM. Let us further assume, for simplicity, that the IGM is at mean cosmic density, the hydrogen neutral fraction varies linearly (from 0 to 1) with distance within the thickness of the I-front, and that the I-front temperature is uniform. The actual value of the I-front temperature depends on the detailed balance between photoheating and cooling processes (see, e.g. Miralda-Escude & Rees 1994). In the following we estimate the expected Ly $\alpha$  signal for a given I-front temperature and medium density<sup>1</sup>. Typical values for this temperature can be inferred from the far-UV spectral indices of QSOs (see e.g., Telfer et al. 2002) and lie in the range  $2 - 4 \times 10^4$  K if the IGM is at mean cosmic density (see e.g., Abel & Haehnelt 1999). At these temperatures we can neglect Ly $\alpha$  emission due to radiative recombinations and write the integrated Ly $\alpha$  flux at the inner edge of the I-front as:

$$\begin{aligned} I_{Ly\alpha} &\simeq \frac{1}{\pi} \int_{I\text{-front}} n_{HI}(r) n_e(r) q_{Ly\alpha}^{\text{eff}}(T) dr \\ &\simeq \frac{1}{\pi} n_H^2 C \chi_e \left( \frac{S}{6} \right) q_{Ly\alpha}^{\text{eff}}(T), \end{aligned} \quad (7)$$

where  $C \equiv \langle n_H^2 \rangle / \langle n_H \rangle$  is the hydrogen clumping factor,  $\chi_e$  the factor that accounts for the contribution of ionized helium to the electron density, and  $S$  denotes the thickness of the I-front. The factor  $1/6$  derives from the integration of  $x_{HI}(1 - x_{HI})$  over the front, while the factor  $1/\pi$  accounts for the angular distribution of the emitted photons (Gould & Weinberg 1996). The actual value of  $S$  depends on several factors, including the spectrum of ionizing radiation  $F_\nu$  and the local density. As a first-order approximation, we can assume that the size of the I-front is given by the mean free path of the ionizing photons with mean frequency  $\langle \nu \rangle = \int_{\nu_0}^{\infty} F_\nu d\nu / \int_{\nu_0}^{\infty} (F_\nu / h_P \nu) d\nu$  (with  $\nu_0$  the hydrogen ionization threshold and  $h_P$  the Planck constant), i.e.  $S \simeq (n_H \sigma_\nu)^{-1}$ , where  $\sigma_\nu$  is the (frequency dependent) photo-ionization cross-section. Substituting  $S$  in equation (7), replacing the hydrogen density with  $n_H = n_{H,0}(1+z)^3$  (where  $n_{H,0}$  is the comoving mean number density), and including the redshift dimming, we obtain the observed integrated surface brightness (SB) in

photons:

$$\Phi_{Ly\alpha} \simeq \left( \frac{f_{\text{esc}} C \chi_e}{6\pi} \right) n_{H,0} \frac{q_{Ly\alpha}^{\text{eff}}(T)}{\sigma_{\langle \nu \rangle}} \quad (8)$$

where  $f_{\text{esc}}$  is the fraction of Ly $\alpha$  photons that manage to escape from the I-front along the line of sight. Remarkably, the observed SB (in photon number) does not depend on the QSO redshift for a given temperature of I-front.

How strong is this signal? The exact value of  $f_{\text{esc}}$  is difficult to estimate as it depends on several factors, including the size of the HII region and the value of the residual HI in proximity of the I-front. Detailed calculations (see §4) suggest that  $f_{\text{esc}} \sim 0.5$ . Typical values of the clumping factor at  $z > 6$ , estimated from simulations (e.g., Gnedin & Ostriker 1997), are of order of  $C \sim 30$ . Therefore, assuming  $\langle \nu \rangle \simeq 3\nu_0$ ,  $\chi_e = 1.2$  and fixing the temperature to  $T \simeq 3 \times 10^4$  K, we obtain:

$$\Phi_{Ly\alpha} \simeq 200 \text{ photons s}^{-1} \text{ cm}^{-2} \text{ sr}^{-1}, \quad (9)$$

at the top of Earth's atmosphere, or, equivalently:

$$SB_{Ly\alpha} \simeq 10^{-20} \text{ erg s}^{-1} \text{ cm}^{-2} \text{ arcsec}^{-2}, \quad (10)$$

for a QSO at  $z \sim 6.5$ .

Although much fainter than the limit fluxes of present-day surveys for Ly $\alpha$  emitters at  $z \sim 6.5$  ( $\sim 10^{-18} \text{ erg s}^{-1} \text{ cm}^{-2}$  for apertures of order of few arcsec<sup>2</sup>; Tran et al. 2004; Kashikawa et al. 2006), the emitting region can cover several hundred comoving Mpc<sup>2</sup>. This corresponds to several hundred arcmin<sup>2</sup> on the sky at  $z \sim 6.5$  and makes the signal detectable with current facilities by means of moderately-high resolution spectroscopy.<sup>2</sup>

Observations of this emission would provide direct evidence for the presence of an I-front, shedding light on the properties of both the ionizing source and the surrounding medium. In particular, as we will show in §5, the angular shape of the apparent I-front can constrain the QSO age and its angular emission properties.

### 3.2. Ly $\alpha$ map of the HI distribution during reionization

Detecting the Ly $\alpha$  emission from the I-front makes it possible to directly map the distribution of neutral hydrogen behind the QSO at the location of the I-front. In fact, the distribution of the Ly $\alpha$  signal on the sky traces the local density of HI as it was before the arrival of the I-front. We will illustrate this with a simple example. Let us consider two patches of the IGM (at mean density) that are simultaneously reached by the QSO I-front. Right before the arrival of the front, one of them is still neutral ( $x_{HI}^a = 1$ ) and the other is significantly ionized ( $x_{HI}^b < 0.1$ ) by a local faint source. Let us further assume that the local source in the second region has a softer spectrum than a QSO and thus that the (initial) temperature of the free electrons is low,  $T \lesssim 10^4$  K. While the I-front crosses the two regions, energetic electrons are released by hydrogen atoms and collisional excite the remaining neutral hydrogen. The Ly $\alpha$  emissivity reaches a maximum at the center of the

<sup>1</sup> The appropriate scaling relations based on other parameters, like the QSO age, ionizing rate and local overdensity will be derived in §5.

<sup>2</sup> The detectability of this signal with present and future instruments will be discussed in §5.2.

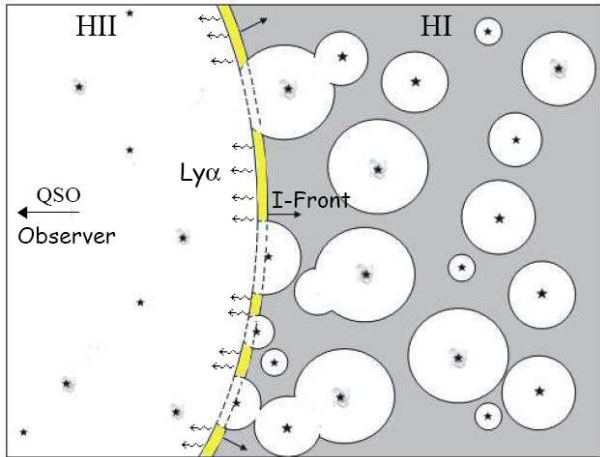


FIG. 2.— This schematic cartoon illustrates how to map the HI distribution using the Ly $\alpha$  emission from the I-front of an high- $z$  QSO. The QSO and the observer are on the left side. The ionizing photons, in the plane of the figure, propagate from left to right and create an I-front wherever they encounter a partially neutral region. Within the I-front, the interactions between neutral hydrogen and the energetic electron released by photo-ionization produce Ly $\alpha$  photons via collisional excitation (yellow stripes). The Ly $\alpha$  emission escapes the I-front through the HII region in the direction of the observer. The regions already ionized by local sources (bounded by the dashed lines) do not produce Ly $\alpha$  via collisional excitations and will appear as holes in the 2-D Ly $\alpha$  map, similarly to a 21-cm tomography. This strictly applies to a young QSO with a relativistically expanding I-front. For older quasars, the entire boundary of the HI region can emit Ly $\alpha$  photons.

I-front where the actual neutral fraction is about  $0.5x_{\text{HI}}$  and the temperature peaks. However, the mean energy of the free electrons and the number density of neutral-hydrogen atoms in the second region are both reduced by a factor  $x_{\text{HI}}^a/x_{\text{HI}}^b > 10$  with respect to the first region: the Ly $\alpha$  emissivity is thus reduced by more than a factor of 100.

A schematic description of how this effect can be used to map the HI distribution is shown in Figure 2 for a uniform IGM. The locally ionized regions will appear as “holes” in the 2-dimensional Ly $\alpha$  map.<sup>3</sup> Given the large angular extension of the HII region, mapping the Ly $\alpha$  emission from the I-front behind a high-redshift QSO can effectively constrain the topology and the history of the reionization process.

#### 4. MODELLING THE Ly $\alpha$ SIGNAL

The rate equations that regulate the temperature and the ionization-fraction profiles inside the expanding I-front cannot be solved analytically. These quantities depend on the local ionizing spectrum that is determined by non-local radiative-transfer (RT) effects. For instance, higher energy photons will be absorbed at higher column densities, causing an effective hardening of the ionizing spectrum at larger distances from the source. Therefore, detailed modelling of the Ly $\alpha$  emissivity requires a full RT transfer calculation for the ionizing radiation.

<sup>3</sup> This strictly applies to young QSOs with I-fronts that are expanding at ultrarelativistic speeds. For older QSOs, the front will move faster in the regions pre-ionized by other local sources and will produce bright Ly $\alpha$  emission from the entire (irregular) boundary of the HI region.

#### 4.1. Continuum Radiative Transfer

To follow the radiative transfer of the continuum ionizing radiation from the QSO, we use a three-dimensional, photon-conserving, and time-dependent code based on a ray-tracing algorithm (Cantalupo & Porciani, in preparation). This code has been developed to study the propagation of I-fronts in cosmological simulations and it includes an adaptive refinement scheme of the computational grids (in space and time) on the front. Among other features, it accounts for the presence of multiple ionizing sources and for the propagation of ionizing radiation produced by recombinations. The time-dependent rate equations include the evolution of HI, HeI and HeII. The gas temperature is computed including the energy input due to photoionizations and collisional ionizations of the three species and all the relevant cooling processes (recombinations, collisional excitations/ionizations, dielectronic recombination of HeII, bremsstrahlung, Compton and Hubble cooling).

For simplicity, in the present study, we consider a single (steady) ionizing QSO surrounded by a uniform (cosmologically expanding) medium. We follow the evolution of the I-front over a few  $10^8$  yr, i.e up to distances of 70-140 comoving Mpc from the source (depending on the QSO luminosity). The adaptive mesh refinement (AMR) scheme allow us to resolve the I-fronts with a large number of (optically-thin) cells of a few comoving kpc at all times. A more general configuration based on the density and velocity fields extracted from a hydro-dynamical simulation will be analyzed in future work.

#### 4.2. Finite light-travel time effects

High-redshift QSOs are expected to produce relativistically expanding I-fronts for an important fraction of their lifetime (Shapiro et al. 2006). This is difficult to follow with most RT codes (see Iliev et al. 2006 for a recent compilation), including our own, in which the ray-tracing algorithm assumes an infinite light speed and ionization fronts tend to propagate faster than light at early times. A quick fix is obtained by limiting the ray-tracing up to a maximum distance but this would lead to the loss of photon conservation. We thus decided to follow a novel approach. For a steady ionizing source in a uniform medium, the correct speed of the I-front at a given radius,  $v_I(r_I)$ , can be expressed in terms of its counterpart obtained assuming an infinite speed of light,  $v_{I,NR}(r_I)$ , by the relation

$$v_I(r_I) = \frac{v_{I,NR}(r_I)}{1 + v_{I,NR}(r_I)/c}, \quad (11)$$

regardless of the difference in physical times at which the I-front reaches the radius  $r_I$  (White et al. 2003; Yu 2005; Shapiro et al. 2006). Therefore, we can get the correct velocity of the I-front by redefining the time variable as follows. We associate to each time step used in the radiative transfer code  $\Delta t_{NR}$  an actual time step  $\Delta t_R$  simply given by:

$$\Delta t_R = \Delta t_{NR}(1 + v_{I,NR}/c). \quad (12)$$

Note that this is an approximate solution, since the optical depth of the photons is still computed at the time of their emission and does not take into account the changes taking place in the medium during their propagation time.

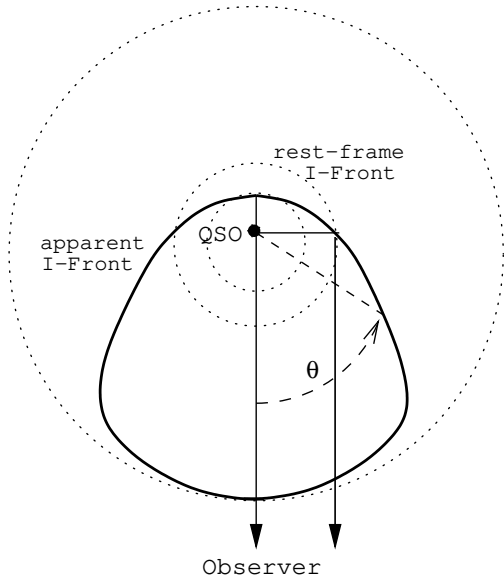


FIG. 3.— Schematic view of the apparent I-front shape (solid line) around an isotropically emitting QSO. The dotted circles represent the I-fronts in the QSO rest-frame at different epochs. The departure from the spherical shape is due to the relativistic expansion speed of the I-front  $c$  combined with finite light-travel effects. The apparent shape is rotationally symmetric along the quasar line of sight. The positions of the apparent and rest-frame I-front coincide for  $\theta = \pi/2$ , while the apparent expansion of the I-front at  $\theta = 0$  is superluminal.

#### 4.3. The apparent evolution of the I-front

The observed shape of the I-front (i.e. the relation between the QSO age,  $t$ , and the I-front distance from the QSO,  $r_I(t)$ , as a function of the viewing angle  $\theta$  defined in Figure 3) will differ from the proper shape because of finite light-travel effects (see equations (1)-(3) in Yu 2005). In fact, the photons we receive from the part of the I-front that is moving towards us travel a smaller distance than the photons emitted behind the quasar.

In Figure 4, we show the time-evolution of the apparent I-front position for three different values of  $\theta$  and  $\langle x_{\text{HI}} \rangle$  (the mean neutral fraction of the medium surrounding the ionization source before the latter turns on). This is the output of a simulation where a luminous QSO (with a total ionizing rate  $\dot{N}_\gamma = 10^{57} \text{ ph s}^{-1}$ , and far-UV energy spectral index  $\alpha = -1.7$ ) turns on at  $z_{\text{in}} = 6.5$  in a uniform medium at mean density with a clumping factor  $C = 35$ . This parameter set is consistent with observations of QSOs showing a GPT at  $z > 6$  (Yu & Lu 2005). From now on, the evolution of the I-front in a fully neutral medium ( $\langle x_{\text{HI}} \rangle = 1$ ) surrounding this source will constitute our reference model.

The time-evolution of the I-front position obtained from our code is in good agreement with the approximate analytical solution by Yu (2005) and Shapiro et al. (2006). For a given QSO ionizing rate, the apparent position of the I-front closest to the observer (red short-dashed line in Figure 4) is very sensitive to both the QSO age and  $\langle x_{\text{HI}} \rangle$ . This is not the case for the apparent position of the Ly $\alpha$  emitting I-front *behind* the QSO (blue long-dashed line in Figure 4), that determines fairly well the QSO age (at least for  $\langle x_{\text{HI}} \rangle \gtrsim 0.1$ ). Combining the information from the Ly $\alpha$  emitting I-front and

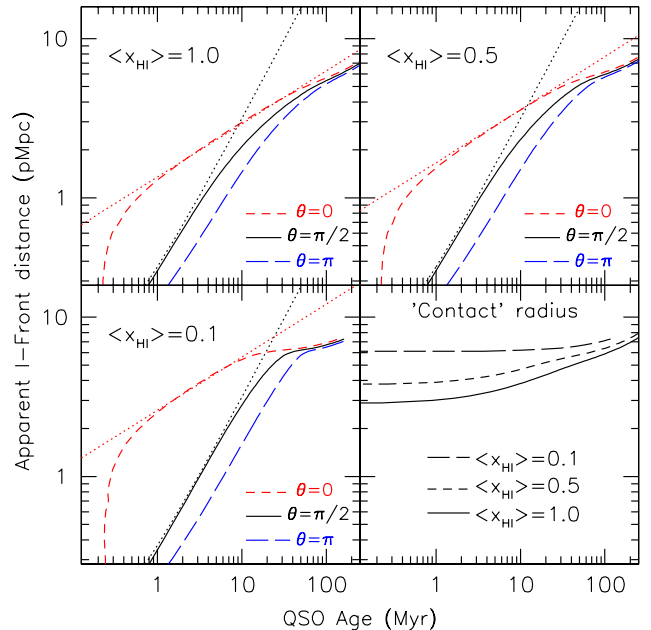


FIG. 4.— Time-evolution of the apparent I-front distance from the QSO (in physical Mpc) as a function of the angle  $\theta$  (defined as in Figure 3) and the mean neutral fraction of the environment ( $\langle x_{\text{HI}} \rangle$ ) (measured before the arrival of the I-front) obtained with our radiative transfer code including finite light-travel effects. Dotted lines are for reference and indicate propagation at the speed of light (black) and  $\propto t^{1/3}$  (red). The bottom right panel shows the evolution of the “Contact” radius, i.e. the position where the I-front closest to the observer ( $\theta = 0$ ) is reached by a photon emitted by the I-front behind the quasar ( $\theta = \pi$ ). Note that the apparent  $\theta = \pi/2$  and the rest-frame I-front expansions are identical. All the panels assume a QSO that turns on at  $z_{\text{in}} = 6.5$  with total ionizing rate  $\dot{N}_\gamma = 10^{57} \text{ ph s}^{-1}$ , far-UV spectral index  $\alpha = -1.7$ , and a clumping factor  $C = 35$ . These parameters are compatible with observed QSOs showing a Gunn-Peterson trough at  $z > 6$  (Yu & Lu 2005).

the position of the GPT in the QSO spectrum, we can significantly constrain both the QSO age and  $\langle x_{\text{HI}} \rangle$ .

At any given time, it is useful to define the “contact” radius ( $R_t$ ) as the position where the I-front closest to the observer ( $\theta = 0$ ) is reached by the photons emitted by the I-front behind the quasar ( $\theta = \pi$ ). This quantity determines the strength of the damping-wing absorption for the observed Ly $\alpha$  signal from the I-front at  $\theta = \pi$ . The evolution of the contact radius for our reference model is shown in the bottom right panel of Figure 4. Note that  $R_t$  keeps nearly constant at early times and grows afterwards. Therefore, even when the rest-frame radius of the HII region is extremely small, the Ly $\alpha$  photons produced behind the QSO (and emitted towards us) will encounter the edge of the ionized bubble when it has grown up to a much larger scale, substantially reducing the damping wing absorption.

#### 4.4. Ly $\alpha$ emissivity from the I-front

Using the time evolution of the I-front derived in the previous section, we want now to compute the Ly $\alpha$  signal produced at given distance (or, equivalently, QSO age) from the central source.

In Figure 5 we show the temperature and ionization profiles for our reference model at two different epochs

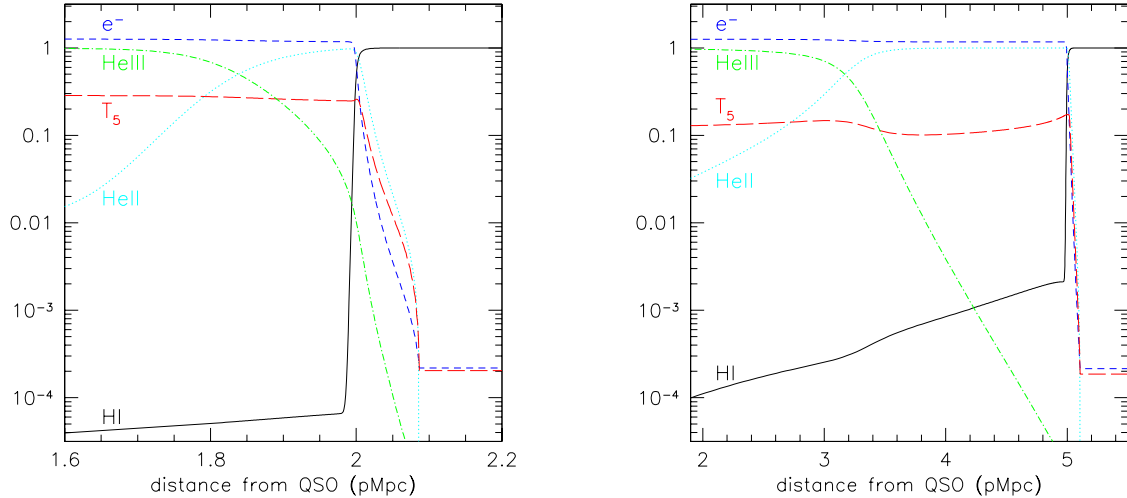


FIG. 5.— Radial (rest-frame) temperature and ionization profiles for our reference model at two different expansion epochs. Solid, dotted and dash-dotted lines respectively show the HI, HeII and HeI fractions. The long-dashed line indicates the temperature expressed in units of  $T_5 = (T/10^5 \text{ K})$ . The short-dashed line represents the ratio  $n_e/n_{\text{HI}}$  which is larger than 1 inside the HII region because of the contribution of partially or totally ionized Helium. Note that the scales and the x-ranges of the two plots are very different.

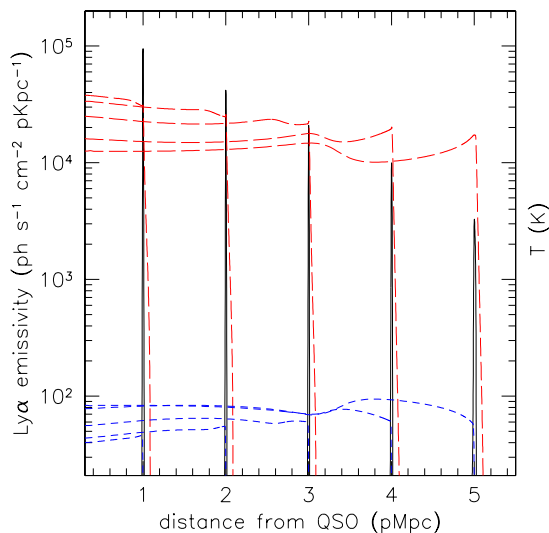


FIG. 6.— Ly $\alpha$  emissivity from collisional excitations (black solid line) and recombinations (blue short-dashed line) for our reference model at different expansion epochs of the QSO I-front. For reference, we also show the evolution of the temperature profiles (red long-dashed line).

in the QSO rest-frame. At early times (left panel), the HII/HI transition is very sharp and the temperature (red, long-dashed line) slowly decreases going outwards until it suddenly drops down in the neutral region. In particular, there is a small peak in the temperature profile at the position of the I-front ( $x_{\text{HI}} \sim 0.5$ , where  $T \sim 3 \times 10^4 \text{ K}$ ) due to the radiative transfer effects that increase the hardness of the ionizing spectrum. The HeII region extends outward of the HII zone, contributing to the free electron density (blue dotted line) and to the temperature. At later stages (right-panel), the HII/HI transition is less sharp and the inner HII region is colder,  $T \sim 10^4 \text{ K}$ . However, the temperature peak at the I-front is more

pronounced, reaching a value of  $T \sim 2 \times 10^4 \text{ K}$ . The HeII region is now well inside the HII zone, with an important effect on the temperature profile (note the temperature drop at  $\sim 3 \text{ pMpc}$ ).

In Figure 6 we show the evolution of the Ly $\alpha$  emissivity from collisional excitations (black solid line), and radiative recombinations (blue, short-dashed line). As expected, Ly $\alpha$  photons generated by collisional excitations are only produced on the I-front, while those produced by radiative recombinations are emitted within the entire HII region. Photons from collisional excitations dominate the total Ly $\alpha$  emissivity, but their contribution diminishes with time as a consequence of the decreasing I-front temperature (red long-dashed line).

#### 4.5. Ly $\alpha$ Radiative Transfer

The density of neutral hydrogen within the I-front is high enough to make the medium extremely optically-thick ( $\tau_{\text{Ly}\alpha} \gtrsim 10^4$  at the line center) to the Ly $\alpha$  photons generated via collisional excitations. Moreover, the residual neutral hydrogen along the line of sight may substantially change the observed Ly $\alpha$  line shape and flux. A numerical treatment of the transfer of resonant line radiation is required to fully account for these effects. We thus compute the observed properties of the Ly $\alpha$  emission from both collisional excitations and radiative recombinations using an updated version of the three-dimensional Ly $\alpha$  Monte Carlo code presented in Cantalupo et al. (2005). In particular, the new version includes two improvements. First, it uses a more precise (and computationally less expensive) analytical fit of the Voigt-Hijertig function proposed by Tepper-Garcia (2006). Second, it performs the line transfer in a medium with a spatially varying temperature. The presence of temperature gradients not only changes the Ly $\alpha$  emissivity but also the shape of the absorption cross-section and thus the scattering process. In particular, a Ly $\alpha$  photon generated in a region with high temperature can more easily penetrate a colder zone before getting eventually absorbed. Thus, the photons produced in the

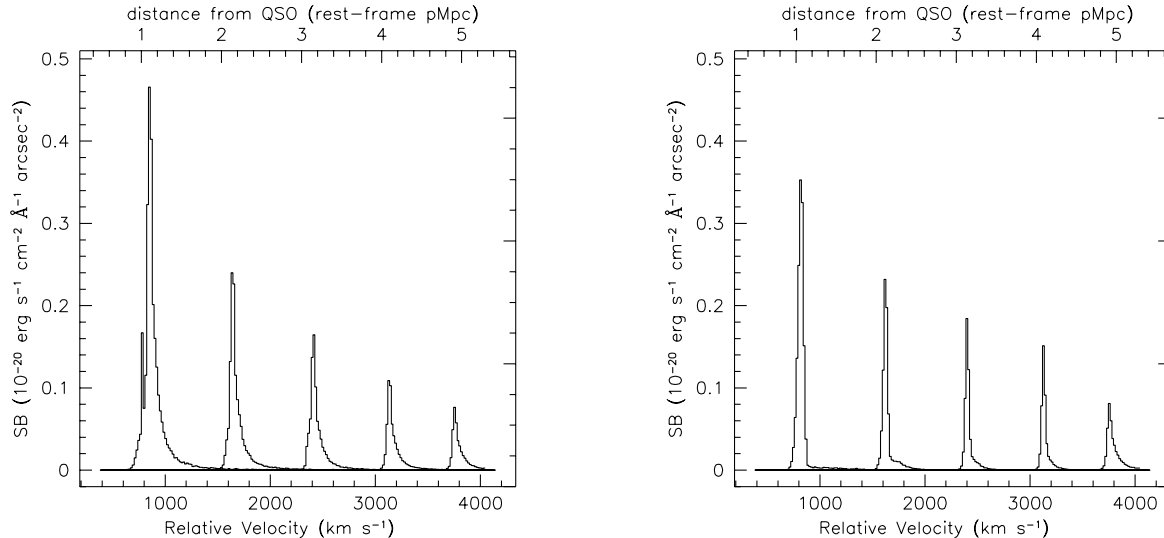


FIG. 7.— Spectral evolution of the Ly $\alpha$  emission from the expanding I-front (behind the QSO) for our reference model. The different lines corresponds to the five different epochs for which the emissivities are shown in Figure 6. The spectra have been obtained with our Ly $\alpha$  RT code for a non-relativistic front (left) and including relativistic expansion (right). Absorption by (residual) HI along the line of sight is included.

(warm) I-front will diffuse more in the neutral (cold) region than expected for a single-temperature medium.

Given the small thickness of the I-front compared with the radius of the HII region, we can work in the plane-parallel approximation. In the absence of Hubble expansion and assuming no absorption from residual HI in the ionized region, the Ly $\alpha$  spectrum emerging from the I-front would be characterized by the symmetric, double-peaked emission typical of plane-parallel, uniform-density media (e.g., Neufeld 1990). In this case, Ly $\alpha$  photons would be emitted with a cosine law over a net solid angle of  $\pi$  (see e.g. Gould & Weinberg 1996). However, both the Hubble expansion and the presence of residual HI increase the number of scatterings for the photons in the blue peak which are then absorbed and re-emitted over a wider solid angle and frequency interval. The net effect is a suppression of the blue peak in the spectrum.<sup>4</sup> The strength of this suppression depends on the residual HI fraction and, therefore, on the I-front distance from the QSO (or, equivalently, on the QSO age). In most cases, the HI residual fraction is high enough to erase the blue peak. On the other hand, the damping wing absorption from HI lying outside the ionized region only reduces the Ly $\alpha$  line flux by a few per cent at all epochs (without altering the line-shape).

In the left panel of Figure 7, we show the evolution of the observed Ly $\alpha$  spectra obtained from the I-front profiles and emissivities presented in Figure 6. At early stages, the blue peak is still detectable but, in general, it is strongly suppressed. Therefore, the emission consists of a single redshifted peak with an asymmetric tail on the red side (i.e. towards the direction of the cold neutral gas). The broadening of the observed peak is

significant compared with the sharpness of the emissivity in Figure 6. Both the suppression of the blue-peak and the damping-wing absorption from external HI reduce the integrated surface brightness with respect to the static, plane-parallel case. Our simulation suggests that the observable integrated SB roughly corresponds to 58 per cent of the ideal case (solid line in Figure 8).

#### 4.6. Ly $\alpha$ Radiative Transfer and Relativistic I-fronts

In the previous section we treated the I-front as static, i.e. we assumed that the Ly $\alpha$  photons leave the I-front on a time scale which is short with respect to the characteristic ionization time of the IGM. This assumption, however, is not valid for young QSOs when the I-front expansion is ultra-relativistic. In this case, as the Ly $\alpha$  photons scatter, the medium becomes optically thinner and the optically-thick edge of the I-front moves outward. If the I-front speed is close to the speed of light, the Ly $\alpha$  photons find themselves inside the HII region after few scatterings. Once there, they will be scattered over a wider solid angle ( $4\pi$  at maximum) with respect to the semi-infinite slab case. Therefore, ultra-relativistic I-fronts should emit a Ly $\alpha$  flux which is reduced by up to a factor of 4 with respect to the static plane-parallel emission and up to a factor of 2 with respect to the non-relativistic case discussed in the previous section.

A full treatment of this effect would require to perform the Ly $\alpha$  RT on a time-evolving grid, with a significant increase of the algorithm complexity and of the requested computational time. However, the fact that the I-front profile shifts in a self-similar way on the relevant time scales gives us the possibility to properly treat Ly $\alpha$  scattering in these extreme conditions. We thus perform the Ly $\alpha$  RT in the rest-frame of the I-front (where the HI density is nearly time-independent). In this reference frame, Ly $\alpha$  photons are preferentially emitted in the direction opposite to the propagation of the I-front. The

<sup>4</sup> This neglects peculiar velocities that, in general, modify the spectral shape of either the red or the blue peak, as shown in Cantalupo et al. 2005.

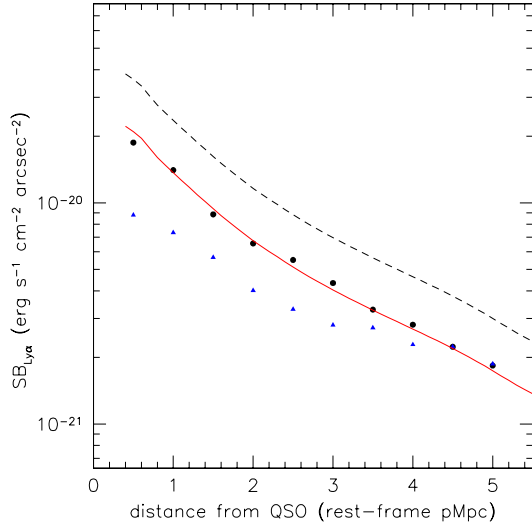


FIG. 8.— Integrated Ly $\alpha$  SB of the expanding I-front (behind the QSO) of our reference model at different expansion epochs, as obtained by our Ly $\alpha$  RT simulations (solid circles). The dashed line represent the expected SB from a plane-parallel (and optically thick) medium given by the integrated Ly $\alpha$  emissivity inside the I-front ( $SB_{\text{Ly}\alpha}^{\text{pp}}$ ). The solid line represent  $0.58 \times SB_{\text{Ly}\alpha}^{\text{pp}}$ . Finally, the solid triangles shows the result of our Ly $\alpha$  RT that includes the effect of the I-front relativistic expansion (see text for details).

resulting time evolution of the line shape and of the integrated SB are shown in the right panel of Figure 7 and in Figure 8, respectively. Both the integrated SB and the line broadening are decreased by a factor  $\sim 2$  during the early stages of the I-front expansion, while they coincide with the non-relativistic results at later epochs. Note that the asymmetry of the line profile is reversed (skewed towards the blue side) at very early times.

## 5. DISCUSSION

The parameters of the ionizing source in our reference model have been chosen based on observations of QSOs showing a GP trough at  $z \sim 6$ . In this case, the Ly $\alpha$  SB produced by the I-front which propagates within a neutral patch of the IGM at mean density always lies between  $10^{-21} - 10^{-20} \text{ erg s}^{-1} \text{ cm}^{-2} \text{ arcsec}^{-2}$  (see Figure 8). How does the Ly $\alpha$  SB change with varying the QSOs and the surrounding medium properties? Moreover, what is the redshift dependence of our results? In order to answer these questions, we performed a series of simulations in which we kept fixed all the parameters of the reference model but one. The resulting SBs (for a neutral patch of the IGM at mean density) are shown in Figure 9. In each panel, we indicate on the top-left the varying parameter (see caption for details) and the reference model is always represented by the black solid line. The SB is obtained from the integrated emissivity and corrected for absorption and RT effects, as described in §4. The correction for the relativistic I-front expansion in the Ly $\alpha$  RT is not included. However, as shown in §4.6, the decrease in the integrated SB is at maximum a factor of 2 when the expansion is ultra-relativistic and it is negligible at later stages.

From the top-left panel in Figure 9, we notice that, for a given QSO age,  $t_Q$ , the expected Ly $\alpha$  SB is roughly

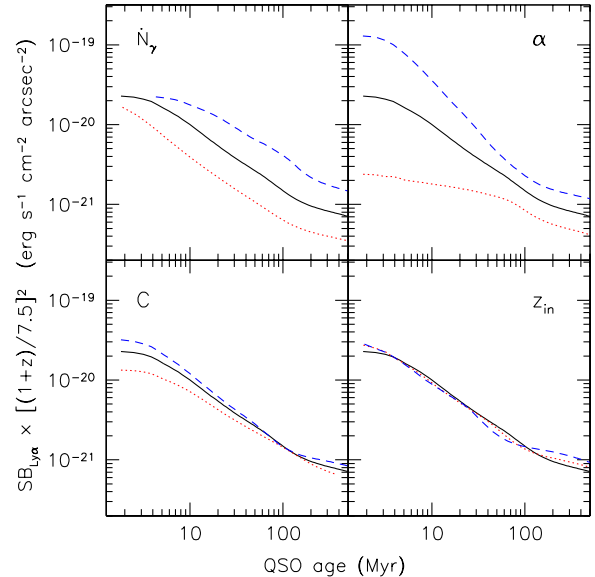


FIG. 9.— Expected Ly $\alpha$  Surface Brightness produced by the QSO I-front as it crosses an initial neutral region of the IGM at mean density. In each panel, the reference model (i.e. total ionizing rate  $\dot{N}_\gamma = 10^{57} \text{ ph s}^{-1}$ , far-UV spectral index  $\alpha = -1.7$ , initial redshift  $z_{\text{in}} = 6.5$ , clumping factor  $C = 35$ ) is represented by the black solid line. The effect of the variation of one parameter with respect to the reference model is shown in each panel with the red dotted and the blue dashed lines representing, respectively:  $\dot{N}_\gamma = 10^{56}$  and  $\dot{N}_\gamma = 10^{58}$  (upper-left panel);  $\alpha = -2.5$  and  $\alpha = -1.0$  (upper-right panel);  $C = 20$  and  $C = 50$  (bottom-left panel);  $z_{\text{in}} = 8$  and  $z_{\text{in}} = 10$  (bottom-right panel). The corresponding SB for a region with initial neutral fraction  $x_{\text{HI}}$  and overdensity  $(1+\delta)$  will scale approximately like  $x_{\text{HI}}^2 (1+\delta)^{1/2}$  (see text for details). Note that the observed SB at very early stages (e.g.,  $t_Q \lesssim 5 \text{ Myr}$  for the reference model) may be substantially lower than the values shown in the figure because of the high-relativistic expansion of the I-front (see text for details).

proportional to  $\dot{N}_\gamma^{1/3}$ , unless the I-front expansion is still ultra-relativistic (i.e.  $t_Q \lesssim 5 \text{ Myr}$  for our reference model). Note that this corresponds to a linear scaling with the ionizing flux at the I-front position. After the ultra-relativistic period, and before recombinations start to play a significant role, the time evolution of the Ly $\alpha$  SB is well represented by a power law ( $SB \propto t_Q^{-1}$ ) independently of the QSO luminosity. The slope of the power law is mainly determined by the spectral index of the QSO spectrum (see top-right panel in Figure 9), as expected by the strong temperature dependence of the collisional-excitation rate. In particular, we found that the SB evolves proportionally to  $t_Q^{-(\alpha+2.7)}$ . Varying the clumping factor ( $20 < C < 50$ ) has little effect on the SB evolution (bottom-left panel in Figure 9). This is because the increase in the collisional excitation rate due to a more clumpy medium is partially balanced by the fact that the medium becomes colder (mainly because of the cooling from collisional excitations themselves). This self-regulation is more efficient as the I-front slows down.

Finally, in the bottom-right panel of Figure 9, we show that the expected  $SB_{\text{Ly}\alpha}$ , for a given  $t_Q$ , decreases proportionally to  $(1+z)^{-2}$  (instead of  $(1+z)^{-1}$  as expected for a medium with fixed temperature, see §3.1). Note that, in order to evidence this relation, the y-axis of the

figure has been properly normalized.

In the models discussed so far we only considered the Ly $\alpha$  SB generated within a neutral patch of the IGM at mean density. As we already shown in §3, the expected emission is proportional to the square of the initial neutral fraction ( $x_{\text{HI}}$ ) (i.e., the medium neutral fraction before the arrival of the I-front). In order to estimate how the expected SB changes with the local overdensity ( $\delta \equiv (\rho - \rho_0)/\rho_0$ ), we performed a series of simulations placing slabs with different values of  $(1+\delta)$  at a given distance from the QSO. We found that, in overdense regions ( $\delta \lesssim 50$ ), the expected Ly $\alpha$  SB is nearly proportional to  $(1+\delta)^{1/2}$ . In summary, assuming  $20 \lesssim C \lesssim 50$ , the Ly $\alpha$  SB produced by a QSO I-front is of the order of:

$$SB_{\text{Ly}\alpha} \sim 10^{-20} \cdot x_{\text{HI}}^2 (1+\delta)^{1/2} \cdot \left[ \frac{t_Q}{10 \text{Myr}} \right]^{-1} \\ \times \left[ \frac{\dot{N}_\gamma}{10^{57} \text{s}^{-1}} \right]^{1/3} \left[ \frac{1+z}{7.5} \right]^{-2} \text{ erg s}^{-1} \text{ cm}^{-2} \text{ arcsec}^{-2}, \quad (13)$$

for  $\alpha \simeq -1.7$ ,  $5 \lesssim t_Q \lesssim 100$  Myr, and  $\delta \lesssim 50$ . Note, however, that QSOs with harder ionizing spectra ( $\alpha \simeq -1$ ) produce significantly brighter I-fronts (blue dashed line in Figure 9).

We do not consider here the Ly $\alpha$  SB produced within more overdense regions. In this case, a proper treatment should also consider hydrodynamical effects. Fluorescent Ly $\alpha$  emission from overdense ( $\delta > 100$ ) regions could be as bright as the I-front emission at mean density. However, these dense regions will appear significantly more compact. An extensive study of the Ly $\alpha$  emission produced by overdense regions and the effect of IGM inhomogeneities will be presented in a future paper (Cantalupo et al., in preparation).

### 5.1. Uncertainties and limitations

For very young QSOs, when the expansion-speed of the I-front ( $v_I$ ) is very close to the speed of light, our model might overestimate the actual Ly $\alpha$  emission. In this case, the photo-ionization time scale ( $t_{\text{ion}}$ ) at the I-front (roughly given by  $t_{\text{ion}} \sim S/v_I$ , where  $S$  is the I-front thickness) can be shorter than the collisional-excitation time scale  $t_{\text{CE}} \sim (C n_{\text{HI}} q(T))^{-1}$ . In our reference model, this effect is important for  $t_Q \lesssim 5$  Myr (and earlier at higher redshifts). In overdense regions the I-front is slower and collisional excitations are faster with respect to the IGM at mean density. Therefore, the Ly $\alpha$  emission produced in these regions is less sensitive to this effect. On the other hand, I-fronts expanding around young quasars lie very close to the source. For instance, the I-front behind a bright QSO at  $z \sim 6.5$  with  $t_Q \sim 5$  Myr appears at a proper distance of 1 Mpc (see Figure 4). If the opening angle of the QSO emission cone is  $45^\circ$  (with respect of the line of sight), the total projected area covered by the I-front will extend over  $\sim 12$  arcmin<sup>2</sup> (or  $\sim 60$  arcmin<sup>2</sup> if the quasar emits isotropically). Therefore, older QSOs provide a larger projected area for detecting the I-front emission and a better constraint on the properties of both the quasar emission and the surrounding IGM. Moreover, older and luminous QSOs produce HII bubbles that are larger than

possible pre-existing ionized regions generated from clustered star-forming galaxies.

Our RT simulations do not consider X-ray radiation produced by the QSO. However, X-ray photons travel unimpeded well beyond the position of the emitting I-front and do not modify the properties of the Ly $\alpha$  signal. In the presence of pre-existing X-ray background, the initial gas temperature will be higher than assumed in our models ( $T \sim 100$  K) and this will slightly increase the Ly $\alpha$  emission from collisional excitations (provided that the medium is still significantly neutral before the arrival of the I-front).

For simplicity, we have assumed a steady ionizing emission rate for the quasars. We also did not account for the possible contribution of other local sources that can change the apparent shape of the QSO I-front and the properties of the surrounding medium (see e.g., Yu 2005; Yu & Lu 2005; Wyithe & Loeb 2007; Lidz et al. 2007). Addressing these effects requires performing high-resolution RT within a fully cosmological simulation and is beyond the scope of the present study.

### 5.2. Detectability

To date, eight QSOs have been detected at redshift  $z > 6.1$  (Fan et al. 2003, 2004; Willot et al. 2007) and all of them have significant ( $\Delta z > 0.1$ ) dark absorption troughs in their spectra in proximity of the QSO redshift. Although this is not necessarily evidence for a surrounding neutral medium, these objects represent the best targets for detecting the I-front Ly $\alpha$  emission.

Let us take, as a practical example, the case of QSO J1148+5251. This quasar has the most accurate redshift measurement ( $z = 6.419 \pm 0.001$ , Walter et al. 2003) and shows complete Ly $\alpha$ -Ly $\beta$  troughs corresponding to an apparent proximity region of  $R_s \sim 5$  physical Mpc (Wyithe et al. 2004, Yu & Lu 2005). Assuming that the medium surrounding the QSO was still significantly neutral ( $\langle x_{\text{HI}} \rangle > 0.1$ ) before the QSO turned on, from the estimated ionizing rate ( $\dot{N}_\gamma \sim 2 \times 10^{57}$  ph s<sup>-1</sup>, see e.g. Yu & Lu 2005) we expect  $8 \lesssim t_Q \lesssim 30$  Myr (see Figure 4). This corresponds, for a QSO spectral index  $\alpha = -1.7$ , to  $0.5 \lesssim SB_{\text{Ly}\alpha} \lesssim 1.5 \times 10^{-20}$  ergs<sup>-1</sup>cm<sup>-2</sup>arcsec<sup>-2</sup> (see equation (13) and Figure 9) for a neutral patch of the IGM at mean density.

Is this signal detectable? Although faint (about 3 orders of magnitude below the sky background), the expected emission may extend over a projected area on the sky up to a few hundred square arcmin. By means of moderately-high resolution spectroscopy ( $R=1000-3000$ ) and integrating the signal over a fraction of the slit length, single neutral patches of the IGM (even at mean density) can be already detected from the ground with current facilities and long integration times ( $T \sim 40$  hr) if they extends over few arcminutes scales (or smaller for slightly overdense regions). For instance, the expected signal-to-noise (S/N) ratio corresponding to the above example and for a ground-based observation (in the atmospheric window at  $\sim 0.9\mu\text{m}$ ) will be of the order of:

$$S/N \sim 7 \times C_f \left[ \frac{D}{8 \text{ m}} \right] \left[ \frac{\zeta}{0.8} \right] \left[ \frac{f}{0.25} \right]^{1/2} \\ \left[ \frac{\Delta_s}{3 \text{ \AA}} \right]^{-1/2} \left[ \frac{T}{40 \text{ hr}} \right]^{1/2} \left[ \frac{\Delta\Omega}{180 \text{ arcsec}^2} \right]^{1/2}, \quad (14)$$

where  $C_f$  is the slit covering factor (i.e. the fraction of the slit where the Ly $\alpha$  emission is present),  $D$  is the telescope diameter,  $\zeta$  the atmospheric transmission,  $f$  the system efficiency,  $\Delta_s$  the spectral bin,  $T$  the integration time and  $\Delta\Omega$  the area of the sky covered by the slit. For a slit width of  $1''$ , the above  $S/N$  implies that we can detect a single neutral patch of the IGM (i.e.,  $C_f = 1$ ) at mean density if it has at least a linear size of  $l \sim 3'$  (corresponding to  $\sim 1$  pMpc at  $z \sim 6.4$ ).

Even if single neutral patches cannot be detected, a proper integration over the total slit length (that can be substantially increased, for instance, using a multi-slit plus filter technique, see e.g., Cantalupo et al. 2007) may reveal at least the position of the Ly $\alpha$  emitting I-front. Once the I-front has been located, we can use its apparent distance from the QSO to determine the QSO age and to constrain the value of  $\langle x_{\text{HI}} \rangle$  (see Figure 4). Possible limitations are given by the unknown opening angle of the QSO emission (that can reduce the projected area over which the I-front may extend) and the difficulties of subtracting the sky lines.

A significant improvement is expected from the next generation of space telescopes like JWST, although the background (i.e., the Zodiacal light) will still be 2 orders of magnitude brighter than the expected signal. With JWST, we will be able to detect single neutral patches of the IGM on smaller scales than allowed from the ground. Moreover observations will not be limited to the narrow redshift ranges permitted by the atmospheric windows. For a given QSO age, the Ly $\alpha$  SB decreases proportionally to  $(1+z)^2$  (instead of the usual  $(1+z)^4$ ). The next generation of space telescopes will thus be able to map HI distribution during the EoR in a broad redshift range.

## 6. SUMMARY AND CONCLUSIONS

We have presented a new method to directly map the neutral hydrogen distribution during the reionization epoch, and to measure the age of the highest-redshift QSOs. We have shown that collisional excitations are an efficient mechanism to produce Ly $\alpha$  photons, even in the low density IGM, provided that nearly 50 per cent

of the hydrogen is neutral and the local temperature is as high as  $T \gtrsim 2 \times 10^4$  K. These conditions are achieved within the I-fronts produced by luminous UV sources, like QSOs, as they expand into the surrounding IGM. The observable Ly $\alpha$  photons are those emitted by the I-front *behind* the QSO (with respect to the observer). These photons can cross the large HII region lying in front of their emission point without being significantly scattered. The emerging signal traces the HI distribution at the location of the QSO I-front (similarly to future 21-cm tomography) since the expected SB roughly scales as the square of the (initial) local HI fraction. The angular distribution of the Ly $\alpha$  emission and its distance from the QSO constrains both the properties of the source (i.e. the QSO opening angle and age) and of the surrounding medium (i.e., the average neutral fraction).

Using detailed radiative transfer simulations that include finite light-speed effects, we have shown that the expected emission appears as a single (broad) line with a width of  $100 - 200 \text{ km s}^{-1}$ . The Ly $\alpha$  SB of a typical QSO I-front that propagates at  $z_Q = 6.5$  within a fully neutral patch of the IGM at mean density lies in the range  $SB_{\text{Ly}\alpha} \sim 10^{-21} - 10^{-20} \text{ erg s}^{-1} \text{ cm}^{-2} \text{ arcsec}^{-2}$ . QSOs with very hard spectra ( $\alpha \sim -1$ ) produce a significantly brighter signal at early phases ( $t_Q \lesssim 10 \text{ Myr}$ ). Interestingly, for a given QSO age, the Ly $\alpha$  SB of the I-front scales as  $(1+z_Q)^{-2}$ .

The signal from neutral patches of the IGM extending over a few arcmin scales is already detectable by current ground facilities with the use of moderately/high resolution spectroscopy. The next generation of space and ground based telescopes will allow us to draw high signal-to-noise maps of the HI distribution with higher angular resolution. Combining this information with a measure of the I-front position, we will be able to simultaneously constrain the reionization history and the emission properties of the highest- $z$  QSOs.

SC is supported by the Swiss National Science Foundation.

## REFERENCES

- Abel, T., & Haehnelt, M. G. 1999, ApJ, 520, L13  
 Baker, J. G., & Menzel, D. H. 1938, ApJ, 88, 52  
 Becker, R. H., et al. 2001, AJ, 122, 2850  
 Bolton, J. S., & Haehnelt, M. G. 2007, MNRAS, 374, 493  
 Cantalupo, S., Porciani, C., Lilly, S. J., & Miniati, F. 2005, ApJ, 628, 61  
 Cantalupo, S., Lilly, S. J., & Porciani, C. 2007, ApJ, 657, 135  
 Fan, X., Narayanan, V. K., Strauss, M. A., White, R. L., Becker, R. H., Pentericci, L., & Rix, H.-W. 2002, AJ, 123, 1247  
 Fan, X., et al. 2003, AJ, 125, 1649  
 Fan, X., et al. 2006, AJ, 132, 117  
 Fan, X., Carilli, C. L., & Keating, B. 2006, ARA&A, 44, 415  
 Furlanetto, S. R., Zaldarriaga, M., & Hernquist, L. 2004, ApJ, 613, 1  
 Furlanetto, S. R., Oh, S. P., & Briggs, F. H. 2006, Phys. Rep., 433, 181  
 Giovanardi, C., Natta, A., & Palla, F. 1987, A&AS, 70, 269  
 Gnedin, N. Y., & Ostriker, J. P. 1997, ApJ, 486, 581  
 Gould, A., & Weinberg, D. H. 1996, ApJ, 468, 462  
 Gunn, J. E., & Peterson, B. A. 1965, ApJ, 142, 1633  
 Haiman, Z. 2002, ApJ, 576, L1  
 Hogan, C. J., & Weymann, R. J. 1987, MNRAS, 225, 1P  
 Iliev, I. T., et al. 2006, MNRAS, 371, 1057  
 Lidz, A., McQuinn, M., Zaldarriaga, M., Hernquist, L., & Dutta, S. 2007, ArXiv Astrophysics e-prints, arXiv:astro-ph/0703667  
 Kashikawa, N., et al. 2006, ApJ, 648, 7  
 Madau, P., & Rees, M. J. 2000, ApJ, 542, L69  
 Madau, P., Meiksin, A., & Rees, M. J. 1997, ApJ, 475, 429  
 Malhotra, S., & Rhoads, J. E. 2006, ApJ, 647, L95  
 Martin, P. G. 1988, ApJS, 66, 125  
 Maselli, A., Gallerani, S., Ferrara, A., & Choudhury, T. R. 2007, MNRAS, 376, L34  
 McQuinn, M., Hernquist, L., Zaldarriaga, M., & Dutta, S. 2007, ArXiv e-prints, 704, arXiv:0704.2239  
 Mesinger, A., & Haiman, Z. 2004, ApJ, 611, L69  
 Miralda-Escude, J., & Rees, M. J. 1994, MNRAS, 266, 343  
 Miralda-Escude, J., & Rees, M. J. 1998, ApJ, 497, 21  
 Neufeld, D. A. 1990, ApJ, 350, 216  
 Oh, S. P., & Furlanetto, S. R. 2005, ApJ, 620, L9  
 Osterbrock, D. E. 1989, University Science Books, 1989  
 Page, L., et al. 2007, ApJS, 170, 335  
 Pengelly, R. M. 1964, MNRAS, 127, 145  
 Santos, M. R. 2004, MNRAS, 349, 1137  
 Shapiro, P. R., & Giroux, M. L. 1987, ApJ, 321, L107  
 Shapiro, P. R., Iliev, I. T., Alvarez, M. A., & Scannapieco, E. 2006, ApJ, 648, 922  
 Songaila, A. 2004, AJ, 127, 2598  
 Spergel, D. N., et al. 2007, ApJS, 170, 377  
 Taniguchi, Y., et al. 2005, PASJ, 57, 165  
 Telfer, R. C., Zheng, W., Kriss, G. A., & Davidsen, A. F. 2002, ApJ, 565, 773  
 Tepper-García, T., & Fritze-v. Alvensleben, U. 2006, MNRAS, 369, 2025  
 Tran, K.-V. H., Lilly, S. J., Crampton, D., & Brodwin, M. 2004, ApJ, 612, L89  
 Walter, F., et al. 2003, Nature, 424, 406

- White, R. L., Becker, R. H., Fan, X., & Strauss, M. A. 2003, *AJ*, 126, 1
- White, R. L., Becker, R. H., Fan, X., & Strauss, M. A. 2005, *AJ*, 129, 2102
- Willott, C. J., et al. 2007, *ArXiv e-prints*, 706, arXiv:0706.0914
- Wyithe, J. S. B., & Loeb, A. 2004, *Nature*, 432, 194
- Wyithe, J. S. B., Loeb, A., & Carilli, C. 2005, *ApJ*, 628, 575
- Wyithe, J. S. B., & Loeb, A. 2007, *MNRAS*, 374, 960
- Yu, Q. 2005, *ApJ*, 623, 683
- Yu, Q., & Lu, Y. 2005, *ApJ*, 620, 31